Atomic electrometry based on heterodyne detection of microwave-induced optical phase shift in a Rydberg medium

Chongwu Xie,[1,2,†] Kang-Da Wu,[1,2,†] Chang-Ling Zou,[1,2] Wei Yi,[1,2] Xinkun Li,[3] Chuan-Feng Li,[1,2] Guang-Can Guo,[1,2] and Guo-Yong Xiang[1,2,*]

[1] *CAS Key Laboratory of Quantum Information, University of Science and Technology of China, Hefei 230026, People's Republic of China*

[2] *CAS Center for Excellence in Quantum Information and Quantum Physics, University of Science and Technology of China, Hefei 230026, People's Republic of China*

[3] *Beijing Institute of Aerospace Control Devices, Beijing 100000, People's Republic of China*

(Received 25 June 2024; revised 23 October 2024; accepted 13 February 2025; published 7 March 2025)

The coherence established in a Rydberg medium through the electromagnetically induced transparency (EIT) process is significantly modified with the inclusion of a microwave (MW) field, leading to a dramatic change in the susceptibility. However, the majority of existing studies focus on the impact of the MW electric field (E-field) on the absorptive properties, while little experimental progress has been made in studying the MW-induced optical phase shift (MIOPS), a feature derived from the MW-dressed refractive index. Here we investigate this coherent effect by measuring the MIOPS of the probe laser in a Rydberg-EIT system in a ^{87}Rb vapor cell. We illustrate the optical phase shift as a function of the MW E-field strength under various conditions and achieve a shift of 0.18 rad in the optical phase (corresponding to a variation of 4.5×10^{-7} in the refractive index) with a MW E-field strength of 8 mV/cm. Moreover, we develop a MW sensor based on MIOPS and achieve a sensitivity of 92.4 nV cm^{-1} Hz$^{-1/2}$ or 279.5 μV cm^{-1} Hz$^{-1/2}$ n^2 when scaling the quantum number n of the Rydberg states. Our experiment demonstrates a promising platform for studying nonlinear quantum optics in a MW-dressed Rydberg medium and opens the avenue for developing next-generation MW electrometry.

DOI: 10.1103/PhysRevApplied.23.034015

I. INTRODUCTION

Quantum coherence between different excitation pathways in an optical medium dramatically changes its macroscopic properties such as the susceptibility of the atomic ensembles, leading to a modified optical response of the medium. Chief among these coherent effects is the electromagnetically induced transparency (EIT) [1], through which one can eliminate the susceptibility of a probe laser at the two-photon resonance. As an emerging quantum technology, the EIT has been applied in a wide range of tasks, such as quantum storage devices [2–4], all-optical switching [5], transistors [6], a velocimeter [7], and optical magnetometry [8].

The EIT has also been proven to be a practically useful technology for Rydberg atoms, where a wide range of fancy and enticing physics can be explored thanks to their distinguished properties. In particular, the large electric dipole moment between Rydberg energy levels offers an ideal interface for linking different regimes of electromagnetic waves: the microwave (MW) and the optical [9]. Recent studies have shown that the inclusion of a MW field in a Rydberg-EIT medium can significantly change the established atomic coherence, leading to a modification in absorptive optical response [10–24]. Based on this effect, a wide variety of applications have been put forward, such as MW-to-optical conversion [10], terahertz imaging [11,12], and MW sensing [13–24].

In contrast to the successes already mentioned, comparatively little experimental progress has been made in investigating the MW-induced modification of the refractive index in a Rydberg medium. In this work, we study the MW-induced optical phase shift (MIOPS) of the probe laser in a hot Rydberg atomic ensemble with an EIT configuration. We experimentally observe a variation of 0.18 rad in optical phase (corresponding to a variation of 4.5×10^{-7} in the refractive index) with a MW electric field (E-field) strength of 8 mV/cm. A more elaborate study regarding the relation between the optical phase shift and the E-field power is carried out. Building on the MIOPS, we develop an electrometry for the detection of MW E-field strength. The frequency of the MW is around 12.6963 GHz, which corresponds a MW transition between Rydberg states $55D_{5/2}$ and $56P_{3/2}$. Specifically, we achieve a sensitivity of 92.4 nV cm^{-1} Hz$^{-1/2}$ or

*Contact author: gyxiang@ustc.edu.cn
†These authors contributed equally.

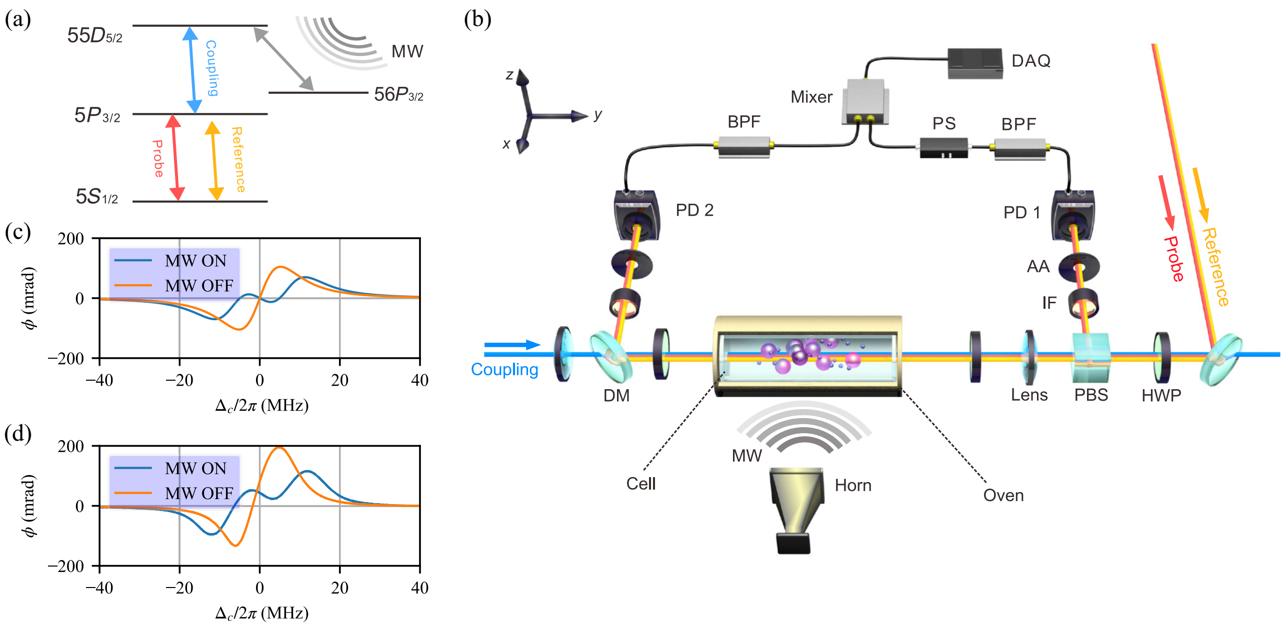

FIG. 1. Experimental setup. (a) Schematic of the experimental setup. The Rydberg-EIT medium is composed of a pure ^{87}Rb vapor cell. The vapor cell is 5 cm in length and 1.25 cm in cross-section radius. It is positioned in a ceramic oven to maintain a stable temperature and facilitate the interaction of MWs with Rydberg atoms. An illustration of the vapor cell and ceramic oven is presented in the Supplemental Material [25]. The probe and reference lasers are overlapped and propagate in the opposite direction to the coupling laser, the beams being incident on separate dichroic mirrors (DM). The MW generated by a horn, positioned approximately 35 cm from the vapor cell, propagates perpendicularly to the direction of the lasers. All lasers and the MW exhibit identical polarization in the z direction. Prior to entering the vapor cell, a half-wave plate (HWP) and a polarizing beam splitter (PBS) divide both the probe and reference lasers into two distinct branches. A branch in the $-x$ direction is identified by a photodetector (PD) designated as PD_1. The adjustable aperture (AA) and the interference filter (IF) settings prior to the PDs are employed to eliminate extraneous light. The alternative branch in the $-y$ direction traverses the cell and is identified by PD_2. The outputs from both PDs are processed through a bandpass filter (BPF) to eliminate the dc component of the signal. A phase shifter (PS) is employed to alter the phase relationship between the outputs of the PDs. A down-conversion mixer is employed to obtain the intermediate frequency output, which is subsequently sampled by a data acquisition system (DAQ) with a maximum sampling rate of 250 kHz. The phase accumulation of the probe laser can be detected by adjusting the PS in such a device. Refer to the Supplemental Material [25] for additional information. (b) Energy levels of the Rydberg-EIT system. The energy difference between the states $|55D_{5/2}\rangle$ and $|56P_{3/2}\rangle$ in the vapor cell is measured to be 12.6963 GHz. (c) Numerical and (d) experimental phase accumulation of the probe laser ϕ versus the coupling laser detuning Δ_c, when the MW is on (blue) and off (orange). When a MW is applied, the original Rydberg state $55D_{5/2}$ undergoes a splitting into two levels within the dressed-state framework, resulting in a dispersion curve that represents the combination of two distinct EIT dispersion curves. The phase ϕ is defined as zero at large detuning, specifically when $\Delta_c/2\pi \approx -40$ MHz. The MW employed in this context is the resonant frequency of 12.6963 GHz, with an E-field strength of approximately 5.4 mV/cm. The curves represent the mean of 20 repeated measurements.

$279.5\ \mu\text{V cm}^{-1}\ \text{Hz}^{-1/2}\ n^2$ when scaling the quantum number n of the Rydberg states, comparable to the state of the art [18,20]. Our research paves the way to a promising platform for investigating Rydberg-mediated nonlinear optics and developing new experimental technology for MW E-field strength sensing.

II. EXPERIMENTAL SETUP AND THEORETICAL MODEL

In a Rydberg-EIT medium, the inclusion of a MW field dramatically alters the atomic coherence, resulting in a change in its optical properties. Here we focus on the modification of the optical phase induced by the MW field. The energy levels used in this work are illustrated in Fig. 1(a). A weak probe laser (red) and a strong coupling laser (blue) couple the ground state $|5S_{1/2}\rangle$ and a Rydberg state $|55D_{5/2}\rangle$ via an intermediate excited state $|5P_{3/2}\rangle$. The inclusion of a MW field (with Rabi frequency $\Omega_{\text{mw}} = d_{\text{mw}}E_{\text{mw}}/\hbar$ and detuning Δ_{mw}) will efficiently shift the Rydberg level. The whole experimental setup is shown in Fig. 1(b). The Rydberg medium used in our experiment is a 5-cm-long ^{87}Rb vapor cell. To stabilize the atom density, the cell is placed in a ceramic oven with a stabilized temperature around 40 °C. A probe laser with a wavelength of around 780 nm (red) and a counterpropagating strong coupling laser with a wavelength of around 480 nm (blue) are overlapped inside the center of the cell. A MW from

TABLE I. Laser parameters. The probe laser remains resonant with the corresponding levels consistently, whereas the reference laser is detuned by 160 MHz. The term "to cell" indicates that the lasers interact with the atomic vapor cell, while "local" signifies that the lasers do not interact with atoms and are detected directly by PD_1. The vector $\hat{e}_k$ represents the direction of laser propagation, whereas the vector $\hat{\epsilon}$ indicates the direction of polarization. Furthermore, all lasers are stabilized to a high-finesse temperature-controlled reference cavity to mitigate phase noise and reduce linewidth.

Lasers	Power	$1/e^2$ radius	$\hat{e}_k$	$\hat{\epsilon}$	Coupling levels
Coupling	80 mW	500 μm	y	z	$\lvert 5P_{3/2}\rangle \leftrightarrow \lvert 55D_{5/2}\rangle$
Probe (to cell)	65 μW	500 μm	$-y$	z	$\lvert 5S_{1/2}\rangle \leftrightarrow \lvert 5P_{3/2}\rangle$
Reference (to cell)	215 μW	500 μm	$-y$	z	$\lvert 5S_{1/2}\rangle \leftrightarrow \lvert 5P_{3/2}\rangle$
Probe (local)	10 μW	...	$-x$	z	$\lvert 5S_{1/2}\rangle \leftrightarrow \lvert 5P_{3/2}\rangle$
Reference (local)	33 μW	...	$-x$	z	$\lvert 5S_{1/2}\rangle \leftrightarrow \lvert 5P_{3/2}\rangle$

a horn antenna propagates in a direction perpendicular to that of the lasers. All the lasers and the MW have the same polarization.

The MIOPS $\Delta\phi$ results from the MW-induced modification of the refractive index: $\Delta\phi = -k_p l \Delta n$, where k_p is the wave number of the probe laser, l is the ensemble length, and Δn is the refractive-index modification induced by the MW. The refractive-index modification process mainly arises from modified atomic coherence established in the MW-dressed EIT medium resulting from the interaction of atomic ensembles between the probe laser, the coupling laser, and the MW E-field, which in quantum mechanical approaches can be derived from the atomic density matrix ρ. The time evolution of the density matrix ρ is governed by the master equation

$$\partial_t \rho = -\frac{i}{\hbar}[H, \rho] + \mathcal{L}[\rho], \tag{1}$$

where H and $\mathcal{L}$ denote the system Hamiltonian and superoperator responsible for relaxation. In our approach, we consider the steady-state solution of the density matrix, $\partial_t \rho = 0$, to interpret the experimental results we present. Here, the susceptibility of the probe light, χ_p, is proportional to the steady-state atomic coherence between states $|5S_{1/2}\rangle$ and $|5P_{3/2}\rangle$, leading to a refractive index, $n_p = \sqrt{1+\chi_p}$. The modification of refractive index, Δn, and therefore the MIOPS $\Delta\phi$, can be determined by comparing the atomic coherence when the MWs are turned on and off. (See the Supplemental Material [25] for more details about the MIOPS simulation.)

We employ the optical heterodyne method [26] to experimentally measure the optical phase of the probe light, utilizing an additional reference laser [orange in Fig. 1(a,b)]. The reference light exhibits a frequency detuning of $\Delta f = \Delta\omega/2\pi = 160$ MHz relative to the probe laser and is coincident with the aforementioned two lasers within the cell. The optical heterodyne method facilitates the extraction of information regarding the optical phase shift $\Delta\phi$, which is embedded in the voltage signals U_{PD_1} and U_{PD_2} oscillating at the beat frequency Δf. Upon mixing and applying a low-pass filter (LPF), the output is expressed as $U_{\mathrm{out}} = T_p \cos(\theta'_{\mathrm{ps}} + \Delta\phi)$, where θ'_{ps} represents an adjustable phase and T_p is a parameter that is proportional to the laser intensity. Additional information regarding the lasers is presented in Table I. Refer to the Supplemental Material [25] for detailed information on phase estimation.

III. RESULTS OF MIOPS

Figure 2 details the theoretical and experimental investigations of the MIOPS effect. The phase shift of the probe laser, $\Delta\phi$, as a function of MW E-field strength E_{mw} with varying MW detunings Δ_{mw} when $\Delta_c = 0$, is presented in Fig. 2(a) for the simulation and in Fig. 2(b) for the experiment. The MIOPS is theoretically zero when $\Delta_{\mathrm{mw}} = 0$ [m2 in Fig. 2(a)]. This can be understood as follows. In the MW dressed-state framework [27], the Rydberg eigenstates split into $|\pm\rangle = (1/\sqrt{2})(|55D_{5/2}\rangle \pm |56P_{3/2}\rangle)$, exhibiting corresponding energy levels of $\pm\hbar\Omega_{\mathrm{mw}}/2$ when $\Delta_{\mathrm{mw}} = 0$. This means that the effective Δ_c for levels $|+\rangle$ and $|-\rangle$ are $-\Omega_{\mathrm{mw}}/2$ and $+\Omega_{\mathrm{mw}}/2$, respectively. The overall susceptibility in the MW-dressed system can be viewed as the sum of the contributions from the two EIT processes: $|5S_{1/2}\rangle \rightarrow |5P_{3/2}\rangle \rightarrow |\pm\rangle$, denoted as $\pm$. The overall MW-modified refractive index is expressed as the average of the refractive indices resulting from the two processes, given by $n = (n_+ + n_-)/2$, where $n_\pm = n_0(\pm\Omega_{\mathrm{mw}}/2)$, and $n_0(\Delta_c)$ represents the refraction in the absence of MW, dependent on the detuning Δ_c. Consequently, the overall optical phase shift is zero, because $n_0(\Delta_c)$ is an odd function around $\Delta_c \sim 0$.

Nevertheless, the nonideal antisymmetry of the dispersion curve observed in our experiment [see the orange curve in Figs. 1(c) and 1(d)] indicates that the phase shift caused by the resonance MW is not experimentally zero [m2 in Fig. 2(b)]. We expect this nonperfect antisymmetry to result from a many-body interaction in the vapor cell (such an interaction can make an asymmetric EIT line shape when the power of lasers and temperature are high enough [20,28–30]). As expected, the MIOPS becomes more pronounced at an appropriate MW detuning [m1 and m3 in Figs. 2(a) and 2(b)], as this condition disrupts

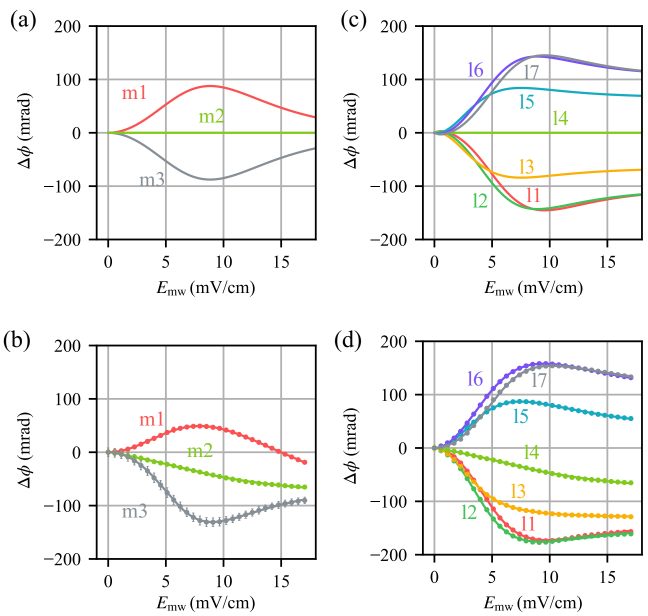

FIG. 2. Experimental results of MIOPS. (a) Theoretical simulation of the MIOPS for various Δ_{mw}, with $\Delta_c = 0$. In this context, m1, m2, and m3 correspond to $\Delta_{mw}/2\pi = 20$, 0, and -20 MHz, respectively. (b) Experimental (dots) and fitted (lines) phase shift of the probe laser, $\Delta\phi$, as a function of MW strength E_{mw} for different MW detunings, under the condition that $\Delta_c = 0$. (c) Theoretical simulation of the MIOPS for various values of Δ_c, with $\Delta_{mw} = 0$. Here l1 to l7 correspond to $\Delta_c/2\pi = 6$, 5, 2, 0, -2, -5, and -6 MHz, respectively. (d) Experimental (dots) and fitted (lines) $\Delta\phi$ as a function of E_{mw} for different Δ_c, when $\Delta_{mw} = 0$. The lines in panels (b) and (d) are fitted using the empirical formula $\Delta\phi = (aE_{mw}^2 + b)/(E_{mw}^4 + cE_{mw}^2 + d) - (b/d)$, with a, b, c, d representing the fitting parameters. A discussion of the formula and the fitting parameters can be found in the Supplemental Material [25]. The error bars in both panels (b) and (d) are the standard deviation of 15 repeated measurements with a 0.1-s integral time.

the symmetry between the two new eigenstates. Nevertheless, a resonant MW will bring the most substantial alterations to the Rydberg levels, and it should be adopted to obtain the most sensitive MIOPS phenomenon. In fact, the MIOPS can be evident with an appropriate and nonzero Δ_c even when $\Delta_{mw} = 0$.

Figures 1(c) and 1(d) illustrate significant alterations in the dispersion curve and a substantial phase shift with appropriate coupling detuning (e.g., $\Delta_c/2\pi \approx 5$ MHz) when a resonant MW is activated. The results presented in Figs. 2(c) and 2(d) indicate a significant MIOPS. For example, l6 and l7 in Fig. 2(d) demonstrate an experimental optical phase shift of about 0.18 rad (corresponding to a variation of 4.5×10^{-7} in the refractive index) with a MW E-field strength of merely 8 mV/cm. The phase shift exhibits saturated behavior, indicating that further increases in the MW E-field strength do not enhance it. The underlying physical concept is that, when the MW is excessively large, the coupling laser experiences significant detuning for the two dressed states $|\pm\rangle$, and leads to weak coupling between levels $|\pm\rangle$ and $|5P_{3/2}\rangle$. Then the Rydberg states exert little influence on the probe laser. Ultimately, the optical phase of the probe laser becomes independent of the MW when the MW is sufficiently large.

TABLE II. Parameters of MWs used in the sensing task. The frequency of the MWs is near the resonant frequency between the levels $|55D_{5/2}\rangle$ and $|56P_{3/2}\rangle$. The resonant frequency measures 12.6963 GHz. The direction of propagation of MWs is denoted by $\hat{e}_k$, whereas $\hat{\epsilon}$ represents the polarization direction. The MW strength is referred to as the strength an atom can experience and is calibrated using Autler-Townes (AT) splitting (see the Supplemental Material [25]). These two MWs are generated by two separate MW sources. Each MW source generates a MW, which are then combined via a MW combiner and linked to a single horn antenna. The beat frequency $\Delta\omega_{mw}/2\pi = 31.111$ kHz should be lower than the response bandwidth of the Rydberg-EIT system, which is approximately several megahertz [16]. The polarization is selected as the same as that of the lasers to ensure all the Rydberg levels can be coupled by the MW [14].

Parameters	Local	Targeted
Frequency (GHz)	12.696300000	12.696331111
Strength (mV/cm)	3.2	···
Coupling levels	$\|55D_{5/2}\rangle \leftrightarrow \|56P_{3/2}\rangle$	$\|55D_{5/2}\rangle \leftrightarrow \|56P_{3/2}\rangle$
$\hat{e}_k$	$-x$	$-x$
$\hat{\epsilon}$	z	z

IV. MICROWAVE ELECTROMETRY

The sensitive relationship between optical phase and MW E-field strength in the MIOPS is applicable for weak MW detection. Experimental determination of the optimal working point is essential for maximizing the performance of MIOPS in sensing tasks, specifically E_{mw} and Δ_c, at the condition where the slope $\partial\Delta\phi/\partial E_{mw}$ is at its peak. The derivative $\partial\Delta\phi/\partial E_{mw}$ attains a maximum value of -36.4 mrad/(mV/cm) at $\Delta_c/2\pi = 5.0$ MHz and $E_{mw} = 3.4$ mV/cm, as indicated by the yellow star in Fig. 3(a).

Thus, we utilize a MW heterodyne technology to detect a small MW signal [16,18] at the point of $\Delta_c/2\pi = 5.0$ MHz and $E_{mw} = 3.2$ mV/cm, which is close to the optimal sensitivity point. An on-resonance local MW field $E_{loc}e^{i\omega_{loc}t}$ is employed to bias the system to the selected working point. A weak target MW $E_{ta}e^{i(\omega_{ta}t+\theta)}$ (to be measured), possessing the same polarization, is combined and directed at the cell. The specifications of both MWs are presented in Table II.

The total MW, which atoms can feel, can be expressed as

$$E_{total}(t)e^{i\omega_{loc}t} \approx \{E_{loc} + E_{ta}\cos(\Delta\omega_{mw}t + \theta)\}e^{i\omega_{loc}t},$$

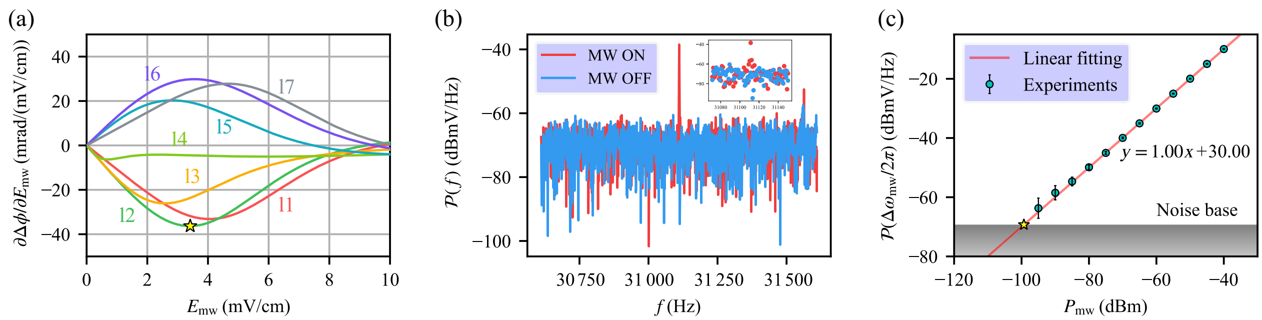

FIG. 3. Experimental results of the MW metrology. (a) The derivatives of the fitting lines presented in Fig. 2(d). The yellow star [3.4 mV/cm, −36.3 mrad/(mV/cm)] represents the maximum point of the slope $\partial\phi/\partial E_{\mathrm{mw}}$. Here l1 to l7 correspond to $\Delta_c/2\pi = 6$, 5, 2, 0, −2, −5, and −6 MHz, respectively. (b) The power spectral density (PSD) $\mathcal{P}(f)$ of U_{out} as a function of frequency, with a targeted MW power of −70 dBm. The sampling time of the DAQ is 1 s. The inset represents an enlarged view. (c) PSD $\mathcal{P}(\Delta\omega_{\mathrm{mw}}/2\pi)$ as a function of the targeted MW power. Here the local and unknown MWs are both near resonance. The gray area, representing the average of $\mathcal{P}_n(\Delta\omega_{\mathrm{mw}}/2\pi)$ across 400 repeated experiments, indicates the noise baseline of our system. The red straight line is fitted by $y = ax + b$. The yellow star represents the intersection of the fitting line and the noise baseline, indicating the minimal detectable MW power of −99.3 dBm. The error bars in the experimental data represent the standard deviation derived from 100 repeated measurements conducted over a consistent measuring duration of 1 s. Here, $\Delta\omega_{\mathrm{mw}}/2\pi = 31.111$ kHz. For a voltage square X (mV^2), it can be expressed in Y (dBmV), with the relationship defined as $Y = 10\log_{10}(X/1\ \mathrm{mV}^2)$.

where $|\Delta\omega_{\mathrm{mw}}| = |\omega_{\mathrm{loc}} - \omega_{\mathrm{ta}}| \ll \omega_{\mathrm{loc}}$ and $E_{\mathrm{ta}} \ll E_{\mathrm{loc}}$ [16]. So, the time-dependent variation of $\Delta\phi(t)$ can be expressed as follows:

$$\Delta\phi(t) = \Delta\phi_{\mathrm{loc}} + E_{\mathrm{ta}} \left.\frac{\partial\Delta\phi}{\partial E_{\mathrm{mw}}}\right|_{E_{\mathrm{loc}}} \cos(\Delta\omega_{\mathrm{mw}}t + \theta), \quad (2)$$

where $\Delta\phi_{\mathrm{loc}}$ denotes the phase shift in the probe laser induced by the local MW. Equation (2) demonstrates that the amplitude of the cosine term in $\Delta\phi(t)$ is directly proportional to E_{ta}, the quantity of interest for measurement. The output signal after the LPF in the MW heterodyne configuration, denoted as $U_{\mathrm{out}}(t)$, is digitally recorded by the DAQ. It is expressed as follows:

$$U_{\mathrm{out}}(t) = T_{\mathrm{p}} \left.\frac{\partial\Delta\phi}{\partial E_{\mathrm{mw}}}\right|_{E_{\mathrm{loc}}} E_{\mathrm{ta}} \cos(\Delta\omega_{\mathrm{mw}}t + \theta), \quad (3)$$

provided that the appropriately selected phase θ'_{ps} fulfills the condition $\Delta\phi_{\mathrm{loc}} + \theta'_{\mathrm{ps}} = \pi/2$. More details on the derivation are shown in the Supplemental Material [25].

A fast Fourier transformation is performed on $U_{\mathrm{out}}(t)$ to obtain the power spectral density (PSD) $\mathcal{P}(f)$. The peak value of $\mathcal{P}(f)$ at the beat frequency $\mathcal{P}(\Delta\omega_{\mathrm{mw}}/2\pi)$ will directly reveal the E-field strength of the target MW. Figure 3(b) presents a typical $\mathcal{P}(f)$ with the MW activated (red) and deactivated (blue), where E_{ta} is about 1.1 μV/cm, corresponding to the peak value of the PSD, $\mathcal{P}(\Delta\omega_{\mathrm{mw}}/2\pi) = -38.5$ dBmV/Hz. The inset in Fig. 3(b) indicates that the 3-dB linewidth of the peak is under 1 Hz.

In Fig. 3(c), the experimentally obtained peak value of the PSD, $\mathcal{P}(\Delta\omega_{\mathrm{mw}}/2\pi)$, as a function of target MW power P_{mw} is shown. The noise base (−69.3 dBmV/Hz) is given by the PSD at $f = \Delta\omega_{\mathrm{mw}}/2\pi$ when the targeted MW deactivated, and such a PSD is denoted by $\mathcal{P}_n(\Delta\omega_{\mathrm{mw}}/2\pi)$. The yellow star in Fig. 3(c), which is the intersection point of the noise base and the linear fitting line, signifies a signal-to-noise ratio of 1 and represents the minimum MW power P_{min} that we can measure ($P_{\mathrm{min}} = -99.3$ dBm). The minimum MW power $P_{\mathrm{min}} = -99.3$ dBm corresponds to a MW E-field strength $E_{\mathrm{mw}} = 92.4$ nV/cm, as determined through AT splitting calibration (see the Supplemental Material [25]). So we can get a sensitivity of $\mathcal{S} = E_{\mathrm{min}}\sqrt{T} = 92.4$ nV cm^{-1} Hz$^{-1/2}$ in our system, with a measuring time of $T = 1$ s. The dipole moment d between states $|nD_{5/2}\rangle$ and $|(n+1)P_{3/2}\rangle$ scales with the quantum number n as $d \propto n^2$ over a broad range of n (see the Supplemental Material [25]). This allows for the rescaling of sensitivity to facilitate a fair comparison with other studies employing different quantum numbers n. The rescaled sensitivity of the system is expressed as $\mathcal{S}_r = \mathcal{S} \times n^2 = 279.5$ μV cm^{-1} Hz$^{-1/2}$ n^2.

V. DISCUSSION

We investigate MIOPS in a Rydberg-EIT medium both theoretically and experimentally. In particular, the relation between the optical phase shift and the MW field is studied, and a phase shift of about 0.18 rad (4.5×10^{-7} in the refractive index) is experimentally achieved using a MW E-field with a strength of 8 mV/cm. The phase modulation reported here is more efficient than the 0.003 rad with a dc E-field strength of about 630 mV/cm reported as the result of $n = 48$ in Figure 3(a) of Ref. [31]. Furthermore, we have developed an atomic MW electrometry based on MIOPS and achieved a sensitivity of $\mathcal{S} = E_{\min}\sqrt{T} =$ 92.4 nV cm^{-1} $\text{Hz}^{-1/2}$.

Based on our theoretical analysis, we expect to achieve more efficient phase modulation, larger phase shift, and better overall sensitivity in the near future. For instance, as shown in the Supplemental Material [25], the efficiency of the phase modulation can be significantly improved with a high-power coupling laser (about 4.1 W), which means we can achieve a sensitivity less than 10 nV cm^{-1} $\text{Hz}^{-1/2}$ in principle. And the MIOPS can be improved to a phase change of 2 rad.

But in our experiment, there are some limits that stop us from further improving the MIOPS, or sensitivity. First, the interplay between Rydberg atoms or ions will become more obvious when the coupling laser is higher. Second, the coupling laser cannot easily improve to several watts. There are some ways to solve these problems. First, we can cool down the vapor to achieve a low atomic density and allow the probe laser to pass through the vapor multiple times. Then we can make the probe laser accumulate a sufficient phase while reducing the density of atoms to avoid the influence of Rydberg interactions. Second, the high-power laser at the wavelength of 480 nm is hard to improve directly, but we can build an optical cavity to enhance its power in the cavity. So, the efficiency of phase modulation and the MIOPS can be further improved in principle. This model itself can be further improved by considering the Rydberg interactions or ion collisions [20,28–30]. We expect this improvement to be able to explain the nonperfect antisymmetry in Fig. 1(c) and the nonzero phase shift of m2 in Fig. 2(b).

Finally, we will examine the differences between the two distinct MW measurement methods, i.e., optical phase measurement and optical power measurement, along with their respective sensitivities. They utilize the real and imaginary parts of the refractive index of the probe light in a Rydberg vapor cell, and the resulting expressions for sensitivity are also similar. Nonetheless, focusing solely on quantum noise for sensitivity is somewhat idealistic, given that technical noise remains the predominant source of noise in our system. The inclusion of technical noise restricts the practical applicability of sensitivity derived solely from shot noise (refer to the Supplemental Material [25] for further details). In practical MW measurement tasks, the system's noise level can be assessed to ascertain whether the primary noise is manifested in optical power or optical phase, thus facilitating the selection of the appropriate measurement method.

ACKNOWLEDGMENTS

We thank En-Long Wang for fruitful discussions. This work was supported by the National Key R&D Program (Grant No. 2021YFA1402004), the National Natural Science Foundation of China (Grants No. 12134014, No. 61905234, No. 62222512, and No. 12374337), the Key Research Program of Frontier Sciences, CAS (Grant No. QYZDYSSW-SLH003), the USTC Research Funds of the Double First-Class Initiative (Grant No. YD2030002007), and the Fundamental Research Funds for the Central Universities (Grant No. WK2470000035).

C.X. and K.D.W. contributed equally to this work. G.Y.X. proposed and supervised the project. C.X. and K.D.W. designed the experiment and the measurement apparatus, constructed the setup, performed the experiment, and collected the data with assistance from G.Y.X. The theoretical derivation was performed by C.X. with assistance from K.D.W., C.L.Z., and W.Y. X.L. produced the atomic vapor cell used in this experiment. The manuscript was drafted by C.X. and K.D.W. with revisions from G.Y.X., C.L.Z., W.Y., C.F.L., and G.C.G.

The authors declare no competing interests.

[1] M. Fleischhauer, A. Imamoglu, and J. P. Marangos, Electromagnetically induced transparency: Optics in coherent media, Rev. Mod. Phys. **77**, 633 (2005).

[2] A. I. Lvovsky, B. C. Sanders, and W. Tittel, Optical quantum memory, Nat. Photonics **3**, 706 (2009).

[3] Y.-H. Chen, M.-J. Lee, I.-C. Wang, S. Du, Y.-F. Chen, Y.-C. Chen, and I. A. Yu, Coherent optical memory with high storage efficiency and large fractional delay, Phys. Rev. Lett. **110**, 083601 (2013).

[4] G. Heinze, C. Hubrich, and T. Halfmann, Stopped light and image storage by electromagnetically induced transparency up to the regime of one minute, Phys. Rev. Lett. **111**, 033601 (2013).

[5] M. Bajcsy, S. Hofferberth, V. Balic, T. Peyronel, M. Hafezi, A. S. Zibrov, V. Vuletic, and M. D. Lukin, Efficient all-optical switching using slow light within a hollow fiber, Phys. Rev. Lett. **102**, 203902 (2009).

[6] M. Mücke, E. Figueroa, J. Bochmann, C. Hahn, K. Murr, S. Ritter, C. J. Villas-Boas, and G. Rempe, Electromagnetically induced transparency with single atoms in a cavity, Nature **465**, 755 (2010).

[7] P.-C. Kuan, C. Huang, W. S. Chan, S. Kosen, and S.-Y. Lan, Large Fizeau's light-dragging effect in a moving electromagnetically induced transparent medium, Nat. Commun. **7**, 13030 (2016).

[8] H. Bao, J. Duan, S. Jin, X. Lu, P. Li, W. Qu, M. Wang, I. Novikova, E. E. Mikhailov, K.-F. Zhao, K. Mølmer, H. Shen, and Y. Xiao, Spin squeezing of 10^{11} atoms by prediction and retrodiction measurements, Nature **581**, 159 (2020).

[9] N. Šibalić and C. S. Adams, *Rydberg Physics* (IOP Publishing, Bristol, 2018), p. 2399, https://iopscience.iop.org/book/mono/978-0-7503-1635-4.

[10] S. Borowka, U. Pylypenko, M. Mazelanik, and M. Parniak, Continuous wideband microwave-to-optical converter based on room-temperature Rydberg atoms, Nat. Photonics **18**, 32 (2009).

[11] C. G. Wade, M. Marcuzzi, E. Levi, J. M. Kondo, I. Lesanovsky, C. S. Adams, and K. J. Weatherill, A terahertz-driven non-equilibrium phase transition in a room temperature atomic vapour, Nat. Commun. **9**, 3567 (2018).

[12] S. Chen, D. J. Reed, A. R. MacKellar, L. A. Downes, N. F. A. Almuhawish, M. J. Jamieson, C. S. Adams, and K. J. Weatherill, Terahertz electrometry via infrared spectroscopy of atomic vapor, Optica **9**, 485 (2022).

[13] J. A. Sedlacek, A. Schwettmann, H. Kübler, R. Löw, T. Pfau, and J. P. Shaffer, Microwave electrometry with Rydberg atoms in a vapour cell using bright atomic resonances, Nat. Phys. **8**, 819 (2012).

[14] J. A. Sedlacek, A. Schwettmann, H. Kübler, and J. P. Shaffer, Atom-based vector microwave electrometry using rubidium Rydberg atoms in a vapor cell, Phys. Rev. Lett. **111**, 063001 (2013).

[15] H. Fan, S. Kumar, J. Sedlacek, H. Kübler, S. Karimkashi, and J. P. Shaffer, Atom based RF electric field sensing, J. Phys. B: At. Mol. Opt. Phys. **48**, 202001 (2015).

[16] M. T. Simons, A. H. Haddab, J. A. Gordon, and C. L. Holloway, A Rydberg atom-based mixer: Measuring the phase of a radio frequency wave, Appl. Phys. Lett. **114**, 114101 (2019).

[17] J. A. Gordon, M. T. Simons, A. H. Haddab, and C. L. Holloway, Weak electric-field detection with sub-1 Hz resolution at radio frequencies using a Rydberg atom-based mixer, AIP Adv. **9**, 045030 (2019).

[18] M. Jing, Y. Hu, J. Ma, H. Zhang, L. Zhang, L. Xiao, and S. Jia, Atomic superheterodyne receiver based on microwave-dressed Rydberg spectroscopy, Nat. Phys. **16**, 911 (2020).

[19] J. S. Otto, M. K. Hunter, N. Kjærgaard, and A. B. Deb, Data capacity scaling of a distributed Rydberg atomic receiver array, J. Appl. Phys. **129**, 154503 (2021).

[20] D.-S. Ding, Z.-K. Liu, B.-S. Shi, G.-C. Guo, K. Mølmer, and C. S. Adams, Enhanced metrology at the critical point of a many-body Rydberg atomic system, Nat. Phys. **18**, 1447 (2022).

[21] C. L. Holloway, N. Prajapati, A. B. Artusio-Glimpse, S. Berweger, M. T. Simons, Y. Kasahara, A. Alù, and R. W. Ziolkowski, Rydberg atom-based field sensing enhancement using a split-ring resonator, Appl. Phys. Lett. **120**, 204001 (2022).

[22] M. Cai, Z. Xu, S. You, and H. Liu, Sensitivity improvement and determination of Rydberg atom-based microwave sensor, Photonics **9**, 250 (2022).

[23] H.-T. Tu, K.-Y. Liao, H.-L. Wang, Y.-F. Zhu, S.-Y. Qiu, H. Jiang, W. Huang, W. Bian, H. Yan, and S.-L. Zhu, Approaching the standard quantum limit of a Rydberg-atom microwave electrometer, Sci. Adv. **10**, eads0683 (2024).

[24] B. Yang, Y. Yan, X. Li, L. Xiao, X. Li, L. Chen, J. Deng, and H. Cheng, Highly sensitive microwave electrometry with enhanced instantaneous bandwidth, Phys. Rev. Appl. **21**, L031003 (2024).

[25] See the Supplemental Material at http://link.aps.org/supplemental/10.1103/PhysRevApplied.23.034015 for details of the simulation of the MIOPS, the methods of phase measurement, E-field calibration, real images of the vapor cell and ceramic oven, the computed dipole moment, and a discussion of the sensitivity in a vapor cell. The Supplemental Material also contains Refs. [13,23,32,33].

[26] A. M. Akulshin, S. Barreiro, and A. Lezama, Steep anomalous dispersion in coherently prepared Rb vapor, Phys. Rev. Lett. **83**, 4277 (1999).

[27] C. Cohen-Tannoudji, J. Dupont-Roc, and G. Grynberg, *Atom-Photon Interactions: Basic Processes and Applications*, Wiley Science Paperback Series (Wiley, New York, 1998).

[28] C. Carr, R. Ritter, C. G. Wade, C. S. Adams, and K. J. Weatherill, Nonequilibrium phase transition in a dilute Rydberg ensemble, Phys. Rev. Lett. **111**, 113901 (2013).

[29] D. Weller, J. P. Shaffer, T. Pfau, R. Löw, and H. Kübler, Interplay between thermal Rydberg gases and plasmas, Phys. Rev. A **99**, 043418 (2019).

[30] D.-S. Ding, H. Busche, B.-S. Shi, G.-C. Guo, and C. S. Adams, Phase diagram and self-organizing dynamics in a thermal ensemble of strongly interacting Rydberg atoms, Phys. Rev. X **10**, 021023 (2020).

[31] A. K. Mohapatra, M. G. Bason, B. Butscher, K. J. Weatherill, and C. S. Adams, A giant electro-optic effect using polarizable dark states, Nat. Phys. **4**, 890 (2008).

[32] S. Barnett and D. Pegg, On the hermitian optical phase operator, J. Mod. Opt. **36**, 7 (1989).

[33] N. Šibalić, J. D. Pritchard, C. S. Adams, and K. J. Weatherill, ARC: An open-source library for calculating properties of alkali Rydberg atoms, Comput. Phys. Commun. **220**, 319 (2017).